RSC Advances

ROYAL SOCIETY OF CHEMISTRY

www.rsc.org/advances

Journal Name

Dynamic Article Links▶

ARTICLE TYPE

Shape Evolution and Size Controlled Synthesis of Mesoporous Hydroxyapatite Nanostructures and their Morphology Dependent Pb(II) Removal from Waste Water

G. Bharath,[a] A. JagadeeshKumar,[b] K. Karthick,[b] D.Mangalaraj,[a] C.Viswanathan,[a] and N.Ponpandian[a]*

ABSTRACT

Nanostructured hydroxyapatite (n-HAp) with tuneable morphologies was successfully synthesized by varying the process parameters using hydrothermal process with CTAB and PEG as surfactant.
10 Systematic experiments were carried out to investigate the influences of process parameters on morphology. The morphology of n-HAp can be modified from nanorods to spheres by replacing the surfactant CTAB with PEG. The prepared materials were characterized by X-ray diffraction (XRD), Fourier transform infrared spectroscopy (FTIR) and field emission scanning electron microscopy (FESEM). The specific surface area (SSA) and pore size were determined by N_2 adsorption-desorption
15 isotherm. The obtained specific surface area of nanorods is more compared to the nanospheres of HAp. These nanostructures of HAp have been used for removalof Pb (II) ions from the waste water. The kinetic mechanism was best described by pseudo-second order models and the isotherm data were fitted well with Longmuir isotherm and Freundlich models. The adsorption of Pb (II) was found to be 714.14 and 526.31 mg/g for the HAp nanorods and nanospheres respectively. The effect of pH, contact time and
20 initial concentration of Pb (II) were also studied through batch experiments.

1. INTRODUCTION

Hydroxyapatite (HAp; $Ca_{10}(PO_4)_6(OH)_2$) is a well-known biomaterial because its chemical composition and structure are similar to that of bones and teeth.[1]It also has excellent
25 biocompatibility, osseointegration and bio stability. Moreover, HAp has been used in numerous applications as scaffolds, chemical sensor, catalyst support, ion conductors, ceramic reinforcement for biomaterials, tissue engineering, bone defect filler, retardant of cancer cells, gene/drug delivery and bio
30 imaging *etc*.[2,3] In particular, n-HAp has been used as an adsorbent for selective adsorption of heavy metals, organic compounds, proteins and DNA molecules.[4,5] Interestingly, the crystalline size, dimensional anisotropy and morphology of these HAp strongly influences theirphysicochemical properties as well as potential
35 applications.[6] Hence, the size and shape controlled synthesis methods of HAp have significant importance. Several methods such as co-precipitation, sol-gel, electrochemical synthesis, hydrolysis, solvothermal and hydrothermal techniqueswere already used for the controlled synthesize of HAp nanoparticles.[7-
40 11] Among all these processes, hydrothermal process is more prevalent due to their high efficiency, large scale, defect free and high crystallinity with moderately controllable morphology.[12] Researchers already reported a hexagonal,prism, elliptical, hierarchical, rod, plate and sphere like morphologies of HAp

45 using hydrothermal process.[13,14] Above all, a soft template was assisting to control the morphologies with uniform size and enhances specific surface area in these preparation methods. The most important soft templates were cetyltrimethylammonium bromide (CTAB), polyvinyl pyrrolidone (PVP), sodium dodecyl
50 sulphate (SDS), 4-aminobenzenesulfonic acid (ABSA) and polyethylene glycol 4000 (PEG -4000). These templates were used to form a rod (1D) and sphere like (0D) n-HAp.[15-17] Hence, CTAB and PEG have been used to control the crystalline size and morphology of n-HAp by suitably varying the cationic and non-
55 ionic surfactants. Normally, the CTAB tune the *c*-axis oriented growth of n-HAp for the formation of well dispersed nanorod like morphology. Meanwhile, the non-ionic PEG influences in the nucleation during the growth process ensuing to control the morphology of nanomaterials. Among the various morphologies
60 of n-HAp, the rod and spheres like morphologies shows high specific surface area (SSA) and pore size distribution and it also shows excellent adsorption capacity of the heavy metals ions, DNA and proteins.[3,18-21] In addition,different morphologies of n-HAp have excellent surface reactivity and adsorption ability
65 depend on the surface charge of HAp. The HAp normally exhibits a hexagonal structure with different charges. Generally, the positively charged calcium is rich on basal plane (*c*- axis) and the prismatic plane (a surface) is hydroxyl and phosphate rich and they are negatively charged.[22] In the adsorption technique,

activated carbon, ferrihydrite,graphene,Fe_3O_4,bismuth and $MnFe_2O_4$@Mn–Co have been reported to be the effective materials.[23-27] Among these, the n-HAp has natural, biodegradable, cost effective, renewable and promising material for efficiently removal heavy metal ions from waste water.

The objective of present study is to obtain the controlled morphology of n-HAp by tuning the hydrothermal process parameters and surfactants CTAB and PEG. The nanorods and nanospheres of n-HAp were prepared by suitably adjusting the surfactants CTAB and PEG. We also explored the possibility of these nanostructures as an adsorbent for the removal of Pb(II) from aqueous solution. The effects of adsorbate pH, contact time and adsorbent dosage on the Pb(II) removal were also explored. The adsorption isotherms were also analyzed based on the Longmuir isotherm and Freundlich model to find the various factors influences on removal. It also explores the adsorption capacity of both nanorods and nanospeheres of n-HAp from the aqueous solution.[19, 28]

2. EXPERIMENTAL SECTION

2.1 Materials

All the reagents used in the present investigations were of analytical/equivalent grade and used without further purification. Calcium chloride dihydrate ($CaCl_2.2H_2O$), Pb(II) nitrate ($Pb(NO_3)_2$), ammonium chloride (NH_4Cl), di-ammonium hydrogen phosphate (($NH_4)_2(HPO_4)$) were obtained from Sigma-Aldrich and N-Cetyl-N,N,N-trimethylammonium bromide (CTAB), poly-ethylene glycol (PEG-6000), ammonium hydroxide (NH_4OH),sodium hydroxide (NaOH), hydrochloric acid (HCl), 4-(2-pyridy1azo) resorcinol (PAR) reagent and ethanol were from Himedia, India.

2.2 Synthesis of Nanostructured Hydroxyapatite (n-HAp) by Hydrothermal Process

In a typical experimental process, 0.059 g of ($NH_4)_2HPO_4$ and 0.5466 g of CTAB were dissolved in 15 ml of aqueous solution with constant stirring. The pH was adjusted to10.5 by adding the ammonium hydroxide (30%). Then, 0.1102 g of $CaCl_2.2H_2O$ was dissolved in 15 ml of deionized water. Consequently, the CTAB-phosphate solution was added drop wise to the calcium chloride solution with vigorous stirring for 30 min. Finally, the translucent mixed solution was transferred to the Teflon-lined stainless steel autoclave. The autoclave was kept in an oven at 160, 180 and 200°C for 24 h and naturally cooled down to room temperature. The supernatant was discarded by decontanation. The resultant white colour precipitate was washed with deionised water and ethanol for three to four times to remove excess ions and impurities present in the suspension. The final precipitate powder was dried under vacuum at 90°C overnight. The diverse morphologies of HAp nanostructures were prepared by varying the concentration between PEG and CTAB like $CTAB_{1-x}PEG_x$(x= 0, 0.25, 0.5, 0.75, 1 mM) with the same preparation conditions.

2.3. Characterization of Materials

The powder X-ray diffraction (XRD) measurements were carried out at room temperature using a PANalytical (X'Pert-Pro) diffractometer with Cu Kα_1 radiation (λ= 1.5406 Å) over a scanning interval (2θ) from 10 to 70°. The average crystallite sizes were estimated using the Scherrer formula. The morphology of the HAp nanostructures was observed by field emission scanning electron microscopy (FESEM) (FEI Quanta-250 FEG) coupled with EDX. The infrared spectrum of the samples was obtained by using Fourier transform infrared (FTIR) spectrometer (Bruker Tensor 27, Germany). UV-Visible spectral analysis was done by using Josco V-650 spectrophotometer. The specific surface areas and pore sizes were determined from BET-N_2adsorption-desorption isotherms using a micromeritics ASAP 2020 surface area analyzer.

2.4. Adsorption Studies

The Pb (II) adsorption isotherm analyses were performed for the different morphologies of HAp nanostructures to determine the optimum adsorption conditions. A typical batch mode adsorption studies were carried out at room temperature. The effect of pH on the adsorption capacity was investigated in the range from 2 to 10 by using Pb (II) solution prepared from the standard 1000 mg/L stock solutions to the preferred concentrations of 10, 20, 30, 40 and 50 mg/L through consecutive dilution. The pH was adjusted by using sodium hydroxide (NaOH) or hydrochloric acid (HCl) solutions. The concentrations of Pb (II) solution wasfixed as 25 mg/L and conduct time between5 to 120 min. The resultant mixture solutions were transferred to 50 ml of standard measuring flask and stirred on a thermostatic mechanical shaker operating at a constant speed of 200 rpm. Finally, the samples were withdrawn from the shaker at predetermined time intervals and the supernatant was collected and centrifuged at 10,000 rpm for 10 min. the resultant clear solution was used to estimate the lead adsorption by using spectrophotometric analysis. The supernatant solution was taken in test tube and added 10 ml of ammonia-ammonium chloride buffer solution (16.9 g of NH_4Cl + 123 ml of liquor ammonia mixed with 250 ml of H_2O) and 1 ml of 0.01 % solution of 4-(2-pyridy1azo)resorcinol (PAR) reagent for spectrophotometric analysis. This solution was incubated at 37 ^{o}C for colour development and finally the absorbance of the samples was measured in a UV-Vis spectrophotometer at the wavelength of 520 nm.[19]

3. RESULTS AND DISCUSSION

3.1. Temperature dependent crystallization and morphologies of n-HAp with CTAB

XRD Analysis:

The effect of hydrothermal reaction temperature on crystallinity and average crystallite size of as-prepared n-HAp were obtained by X-ray diffraction analysis. The high intensity and sharp peaks in the XRD pattern in Fig. 1 confirms the high purity and crystallinenature of n-HAp prepared by different hydrothermal reaction temperatures of 160, 180, and 200°C for 24h with CTAB as surfactant.The obtained diffraction peaks were very well matches with the standard [JCPDS # 09-0432]. There is no impurity phases were present in the prepared samples. Few important peaks were appears at an angle (2θ) of 26.2, 32.1, 32.5, 33.2 and 34.3^o corresponding to the planes of (002), (211), (112), (300) and (202) respectively.
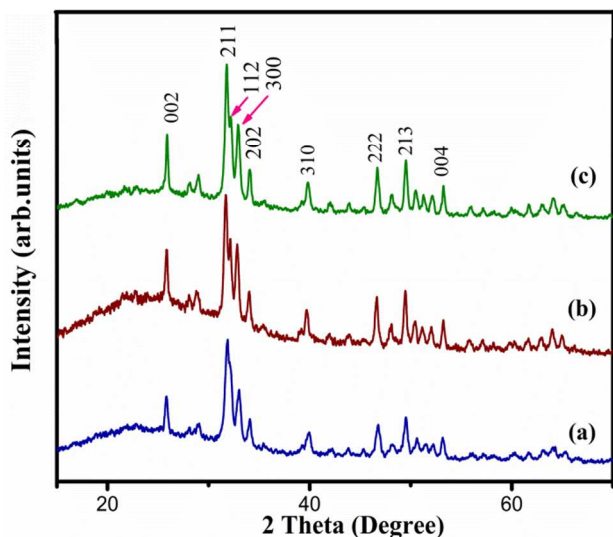
Fig.1 XRD pattern for the as-prepared HAp prepared with CTAB for different hydrothermal reaction temperatures of (a) 160, (b) 180 and (c) 200°C for 24 h.

[5] The peaks at 26.2 and 32.1^{o}shows high intensity corresponds to (002) and (211) planes of n-HAp.The intensity of the diffraction peak increases by increasing the reaction temperature to 180 and 200 ^{o}C and it confirms the improved crystallinity of the n-HAp. The average crystallite sizes estimated by using Scherrer formula [10] were 56, 61 and 67 nm for the 160, 180, and 200°C for 24h hydrothermal reaction. The results confirm the n-HAp was composed of small grains with good crystallinity.

FTIR Analysis:

[15]   The formation and identification of the functional group of the HAp were further supported by the FTIR analysis. The FTIR spectrum in Fig. 2shows theintensed peak at 3439 and 1637 cm^{-1}corresponds to the bending mode of H$_2$O, the characterize absorption band of the OH$^-$stretching mode occurs at 3574 and [20] 632 cm^{-1} .
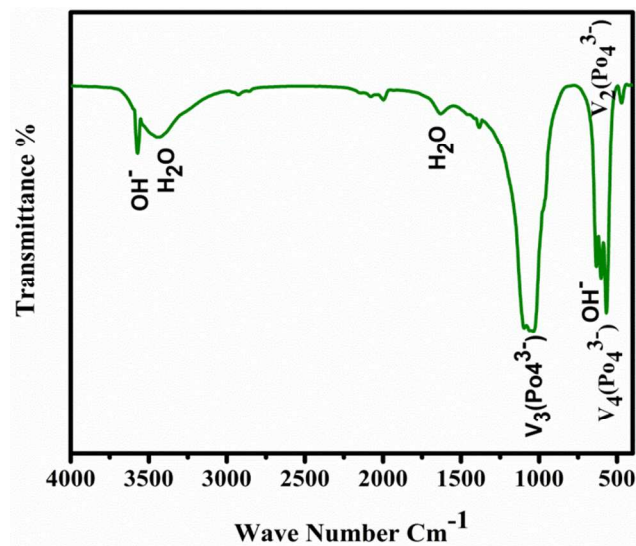

Fig.2 FTIR spectrum for the as-prepared HAp nanorods

The asymmetric stretching vibrations of the P-O in the PO$_4$$^{3-}$ groups were located at 1099 and 1037cm^{-1}. The intense peak at

[25] 568 and 601 cm^{-1}were due to the bending vibrations of the O-P-O in the PO$_4$$^{3-}$groups.[5]
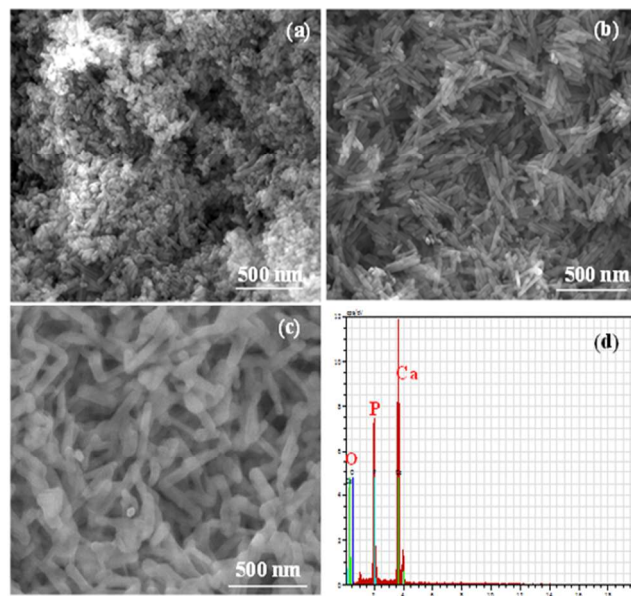

Fig.3 FESEM images for the as-prepared n-HAp with different hydrothermal reaction temperatures of (a) 160, (b) 180, (c) [30] 200°C and (d) EDX spectrum.

Morphological Analysis:

    The morphology of the n-HAp was investigated by using field emission scanning electron microscopy (FESEM). Figure 3 provides the morphologies for three different hydrothermally [35] treated samples and it clearly shows the marked difference between the surface morphologies.It shows the rod like morphology for all the samples with different length and diameter based on the hydrothermal reaction temperatures.Figure 3a shows the rod-like morphology for the n-HAp hydrothermally reacted at [40] 160 ^{o}C for 24 h in the presence of CTAB. The rods have a length and diameter of 64 and 23 nm respectively. The 180 ^{o}C hydrothermally treated sample consists of rods with uniform size distributions with increased dimension as shown in Fig. 3b. A significant increase in the length and diameter of the nanorods [45] were observed with the size of 420 and 65 nm respectively.The average length and diameter of the nanorods were further increases to 550 and 100 nm respectively with irregular shapes by increasing the growth temperature to 200°C as shown in Fig. 3c. Figure 3d shows the EDX spectrum for the n-HAp to examine the [50] elemental composition and it confirms the presence of Ca, P and O species without any impurities.

Formation Mechanism:

The schematic illustration in Fig.4 explains the possible formation mechanism of n-HAp nanorods with different growth [55] temperatures in the presence of CTAB. The formation of n-HAp happens in two stages as nucleation and growth. The nucleation process was same for all the samples but the temperature influences the growth of nanorods.[29-33]The morphological evaluation can be influenced by the growth temperature and the [60] cationic surfactant CTAB. The CTAB influences the formation of rods like morphology and increases the crystallization process.[34] During the growth process cationic CTAB was dissolved completely in deionized water and form the spherical shaped
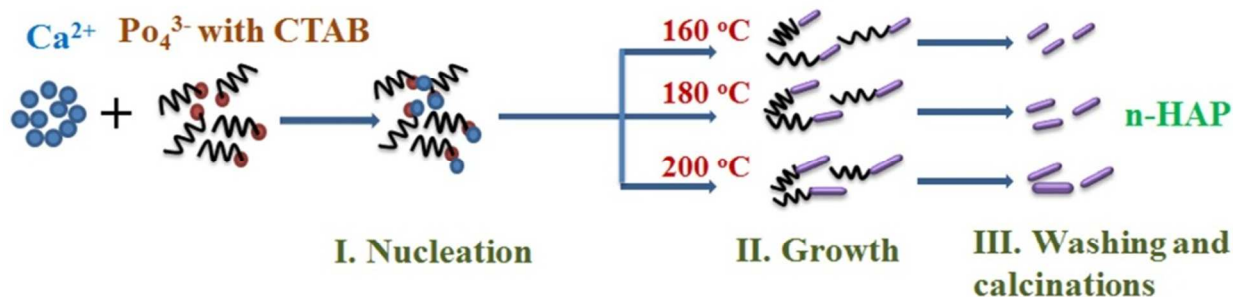
Fig.4 Schematic illustration of temperature dependent and surfactant assisted nucleation and growth mechanism of n-HAp.

micellewith the critical micelle concentration (CMC) of below 1 mM in aqueous solution. Above the CMC, the spherical shapes of micelles were elongated to form the rod like morphology of n-HAp. In general, the CTAB releases a cation with tetrahedral structures and forms the rod shaped micelle and NH_2PO_4releases phosphate anions with tetrahedral structure. The phosphate anions were attached with the CTAB cationic molecules. Finally, the nucleation and growth started along the *c*-axis with the addition of Ca^{2+} solution leads to the formation of rod shaped HAp nanostructures.[35]

The hydrothermal reaction temperature plays a vital role in the formation of morphologies and crystallinity of the n-HAp. The growth of n-HAp nanorods were occurs due to the initial critical nuclei size, saturation ratio, dissolution and recrystallizationprocess. The solubility is higher during the thermodynamic equilibrium by increasing the temperature thereby more number of nuclei was dissolved. So the size of the critical nuclei increases, thereby the size of the nanorods were also increasesdue to the increase in growth temperature.[13]The driving force decreases while the volume energy increases during the increase of growth temperature to 180 °C.Thereby the solubility and number of nuclei increases and it may be the reason for increase in the size of n-HApnanorods.[36] Further increase the temperature to 200°C, the structure of the rod shaped CTAB micelles were breakdown and it forms an uneven shaped n-HAp nanorodsand it was observed through FESEM image as shown in Fig. 3c.The results and the mechanism explain the role of hydrothermal reaction temperature and CTAB on the formation of different morphologies of n-HAp. Further, the n-HAp nanorods prepared at 180°Cshows smooth surface with uniform size and well crystalline nature. Consequently, the morphologies of the n-HAp were further improved by preparing the sample with the constant reaction temperature of 180 °C for 24 h by tailoring the other hydrothermal parameters.

3.2. Effect of PEG substitution for CTAB and their morphological evaluation

XRD Analysis:

The n-HAp with different morphologies was also obtained by gradually varying the molar ratio of PEG and CTAB. The molar ratios of $CTAB_{1-x}PEG_x$ ($x=$ 0, 0.25, 0.5, 0.75, 1 mM) and then subjected to a hydrothermal treatment of 180 °C for 24h. Figure 5 shows the X-ray diffraction pattern for the as-prepared n-HAp samples. All the peaks in the diffraction pattern demonstrate the pure hexagonal structure of the HAp and it matches very well with the standard (JCPDS #. 09-0432). Figure 5(a) shows the XRD pattern for the n-HAp prepared with CTAB and it shows the strong and sharp peaks along (002) and (211) plane. The estimated averagecrystallite size was 23 nm by using the Scherer formula. The addition of PEG (0.25, 0.5, 0.75mM) by partially replacing the CTAB, the intensity of the diffraction peak and the crystallinity decreases as shown in Fig.5(b-d) due to the decrease in the average crystallite size to 61, 48 and 27 nm respectively. Figure 5 (e) shows the XRD pattern for the n-HAp prepared with 1mM of PEG-4000. It shows the broad diffraction peaks and reduced intensity and the average crystallite size estimated was 15 nm.
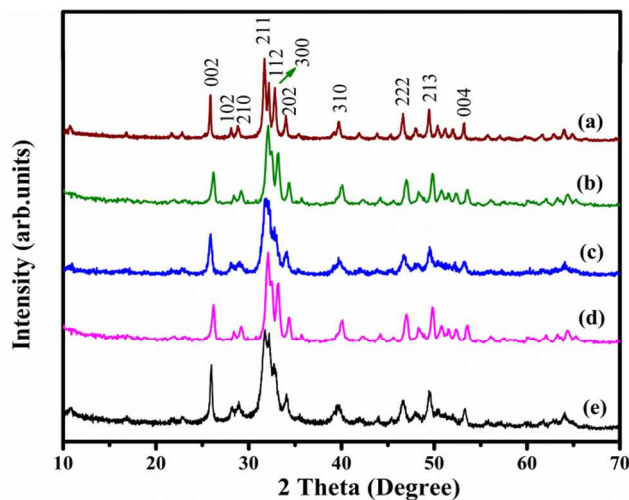

Fig.5 X-ray diffraction pattern for the n-HAp prepared with different molar ratio of CTAB and PEG(a) 0, (b) 0.25, (c) 0.5, (d) 0.75 and (e) 1.0mM of PEG.

Morphology Analysis:

The morphology and dimension of the as-prepared n-HAp crystals were obtained by using FESEM. The images of the n-HAp prepared by varying the ratio of CTAB and PEG with the reaction temperature of 180°C for 24 h were shown in Fig. 6 (a)-(e). Figure 6(a) shows the morphology of the n-HAp, prepared with 1 mM of CTAB as surfactant. It shows the well dispersed nanorods of n-HAp with an average diameter and lengthof 30 and 250 nm respectively. The addition of different concentrations of PEG (0.25, 0.5 and 0.75 mM) by replacing the part of CTAB in the synthesis procedure fascinatingly changes the morphologies such as spindle, rice and spherical as shown in Fig. 6(b) - (d).
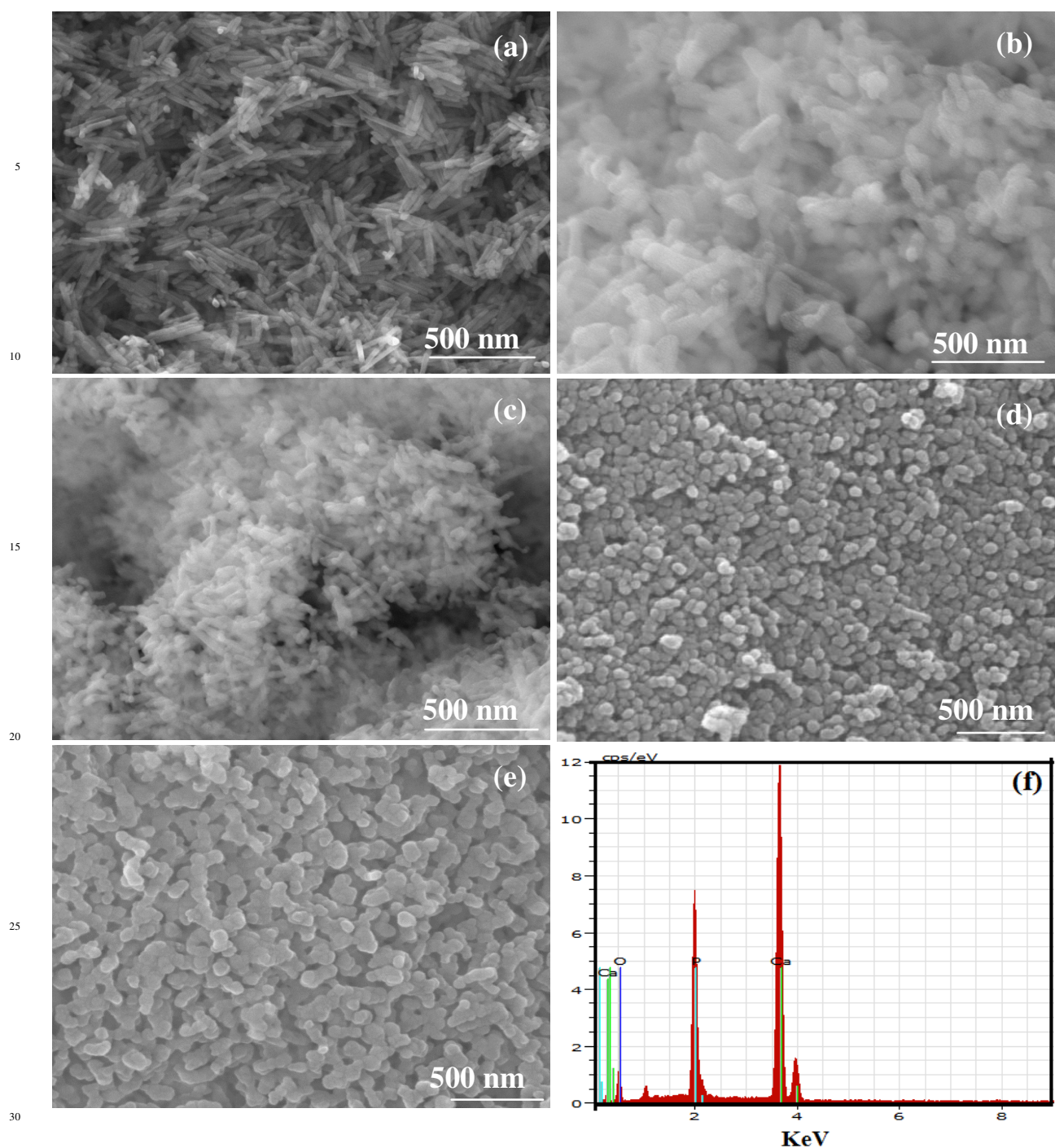
Fig.6 FESEM images for the n-HAp prepared with different molar ratio of $CTAB_{1-x}PEGx$ with x as (a) 0, (b) 0.25, (c) 0.5, (d) 0.75 and (e) 1.0 mM of PEG and (f) EDX spectrum.

The spindle like n-HAp in Fig. 6b shows the diameter and length of 80 and 200 nm respectively. Whereas the rice like n-HAp shows the diameter and length of 20 and 80 nm. The sphere like morphology shows an average diameter of 45 nm.

Figure 6e shows the chain like n-HAp with the combination of nanospheres with the diameter and length of the 20 and 180 nm respectively for the 1mM of PEG. The schematic diagram in Fig.7 shows the morphological evolution by altering the molar ratio between CTAB and PEG. The sphere like micelle formed when the CTAB concentration was below the critical micelle concentration (CMC) of 0.9 Mm. The rode like n-HApwasobtained by 1 mM of CTAB because of theCMCwas above 0.9 mM.[29,30] During thisconcentration the sphere like micelles were elongated to rods like micelles to form the rod shaped n-HAp.

Formation Mechanism:

The change in the molar ratio $CTAB_{1-x}PEGx$ with x=0, 0.25, 0.5, 0.75, 1 changes the morphology of n-HAp. The nanorod like

morphology was observed in the case of n-HAp prepared only with CTAB as surfactant. The substitution of PEG with different molar ratios instead of CTAB changes the rod shapes to spindle, rice and spherical like structures with reduced size and shape. The morphological evaluation of n-HAp can be influenced by two folds. First, the drastic decrease in the CTAB concentration reduces the critical micelle concentration (CMC). According to micellar growth mechanism, there is a decrease in the internal driving force initiates the formation of small aggregates with smaller size and shape of n-HAp.[37] Further the PEG being a non-ionic surfactant and it can act as a co-template during the crystallization and the nucleation process. In addition, the increasing concentration of PEG gradually reduces the initial aggregation of nucleation thereby it requires long time to produce large aggregation of nucleation resulting smaller crystallite size. This confirms the surface structure and size of the n-HAp was controlled by the addition of PEG.
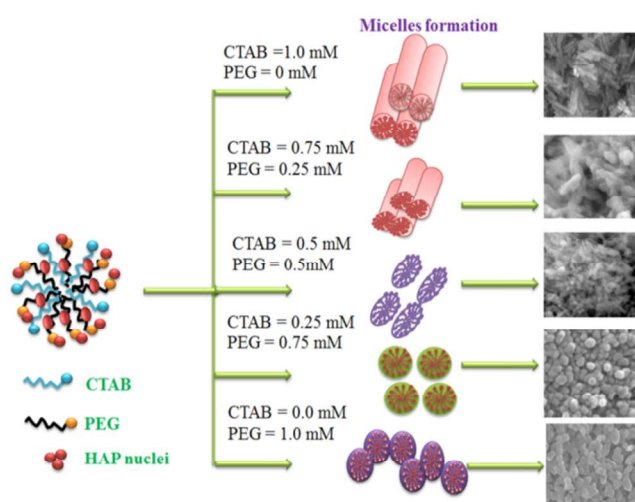

Fig.7 Morphological evaluation of n-HAp by changing the molar ratio of the CTAB and PEG(0, 0.25, 0.5, 0.75, 1 mM of PEG)

Surface Area and Pore Size Determination:

Specific surface area and porous nature of rod and sphere like n-HAp were further investigated by nitrogen physisorption (adsorption/desorption) isotherms. Figure 8 (a) and (b) shows the N_2 adsorption - desorption isotherms for the nanorods and nanospheres respectively. It exhibits a type IV isotherm at a relative pressure (p/p_o) between 0.1 to 0.9, representing the mesoporous structure of n-HAp. A Barrett-Joyner-Halenda (BJH) calculation reveals the average pore size distribution is in the range of 8 and 6 nm treasured for the rod and sphere like n-HAp. The specific surface area (SSA) for the rod like n-HAp can be obtained as 97 m^2g^{-1}, which is much higher than the sphere like n-HAp of 75 m^2g^{-1}. This value is similar to the already reported SSA for the mesoporous n-HAp of 87.3 m^2g^{-1}.[3,18] The high specific surface area of n-HAp is due to their small crystal/grain size as observed from FESEM and XRD respectively.

3.3. Pb(II) Adsorption

Hydroxyapatite is a well-known and an effective adsorbent to remove hazardous materials and heavy metals from waste water. The present study is to investigate the morphological dependent Pb (II) adsorption ability from waste water by using both HAp nanorods and nanospheres. The removal efficiency was studied by varying the parameters such as pH, contact time, and initial concentrations of the metal ions. All these parameters were optimised and find out the removal efficiency of Pb (II) ions from aqueous solution.

Effect of pH:

The pH is one of the most important parameters for the adsorption of heavy metals from aqueous solutions. In this study, the adsorption of Pb^{2+} ions on HAp nanorods and nanospheres were investigated with the range of pH from 2 to 10
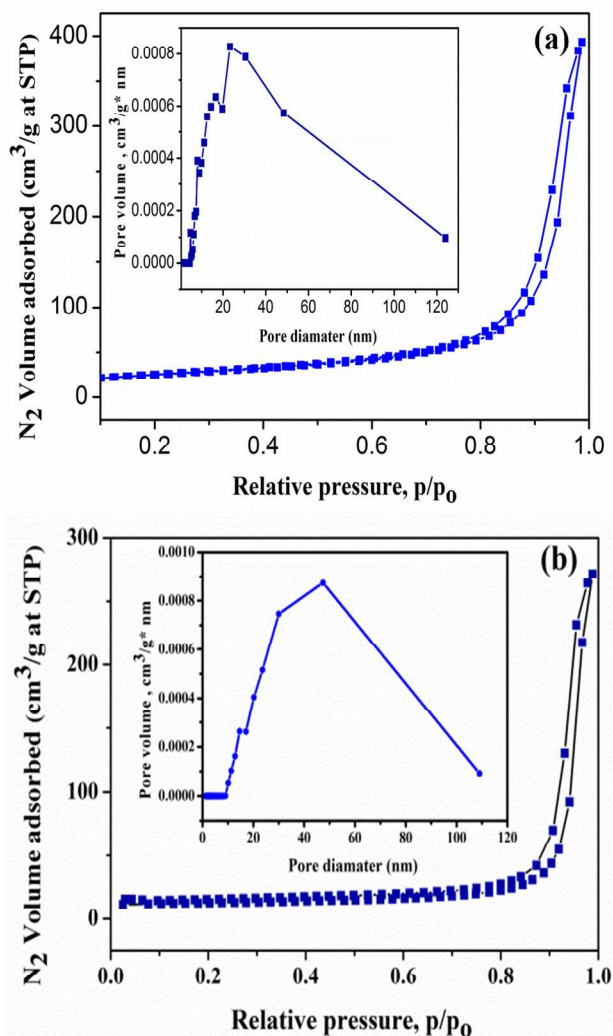

Fig.8 The N_2 physisorption (adsorption/desorption) isotherms and pore size distributions of hydroxyapatite (a) nanorods and (b) nanospheres.

by fixing the concentration of adsorbent dosage to 10 mg/L for the different initial concentrations of adsorbate as 20 to 100 mg/L. The Pb(II) adsorption efficiency was studied for n-HAp nanorods and nanospheres with different initial concentrations of the adsorbate. The result shows the adsorption capacities of Pb (II) increases significantly with the increase of pH from 2 to 4 and there is a small decrease with plateau at the pH range of 4 - 10. The adsorption maximum was observed as 97.5 and 90.5 % for the n-HAp nanorods and nanospheres at pH 4 for initial concentration of 20 mg/L of Pb (II). Similar reports were already reported for adsorption of Pb (II) ions on HAp.[33-36] Also, the adsorption percentage of Pb (II) decreases by increasing the
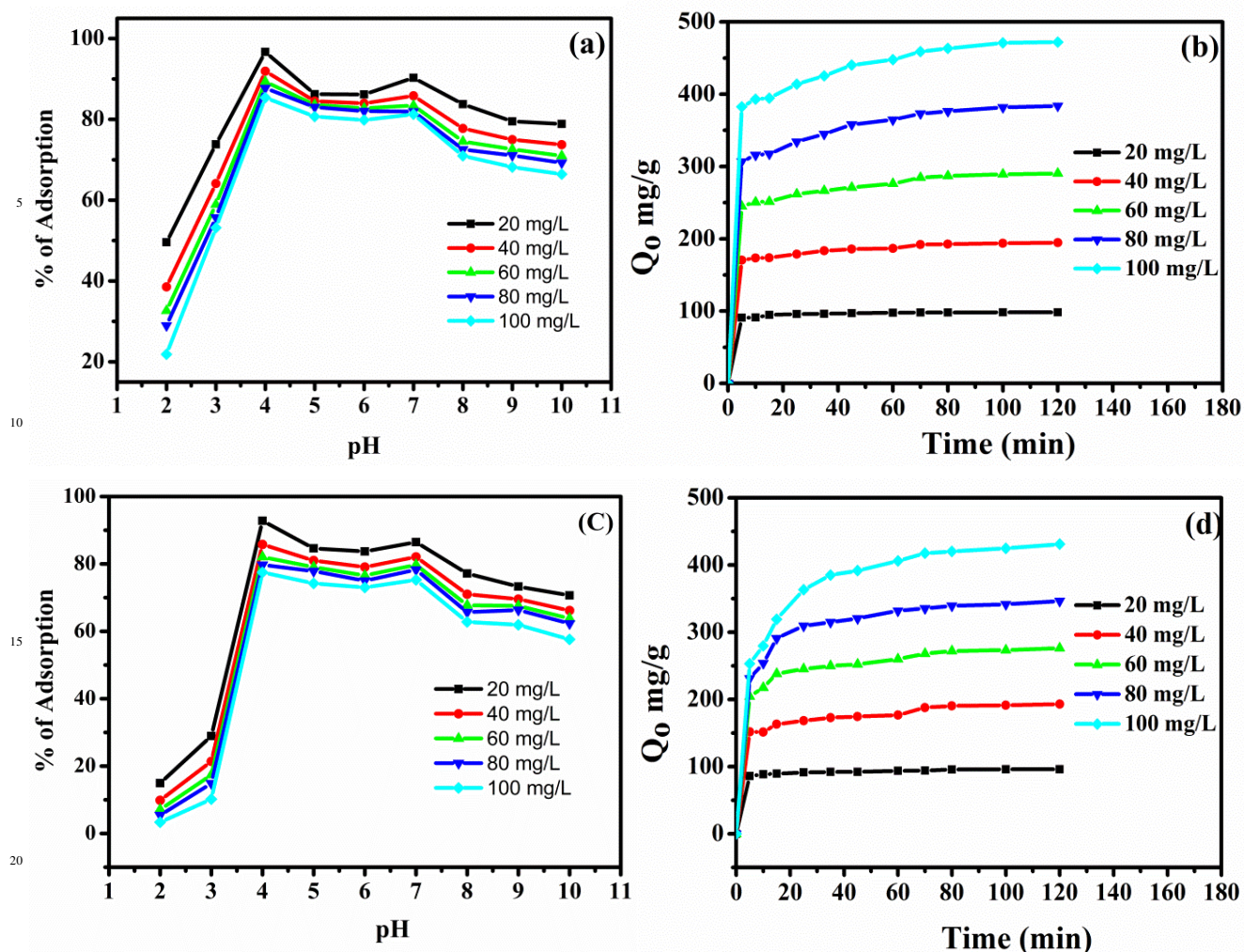
Fig.9 Adsorption effect of pH and contact time on the Pb(II) with different initial concentrations (20 to 100 mg/L). Dosage of adsorbent is 10 mg/g (a) and (c) effect of pH, (c) and (d) effect of contact time of the hydroxyapatite nanorods and nanospheres respectively.

initial concentration from 20 to 100 mg/L. At lower initial concentrations the adsorption percentage of Pb (II) was higher due to the larger specific surface area and more adsorption sites. The higher initial concentration of Pb (II) ions decreases the adsorptions site and specific surface area and therefore the removal percentage of the adsorbate decreases.[34] Since the optimum pH for Pb (II) adsorption by n-HAp was found to be 4 and this pH has been used for further studies.

Contact Time:

The effects of contact and equilibrium times are most important parameters for the adsorption of heavy metal ions from aqueous solutions. Figure 9 (b and d) shows the effect of contact time between 5 to 120 min for the adsorption of Pb(II) ions by n-HAp nanorods and nanospheres with different initial concentrations from 20 to 100 mg/L with a pH of 4. The equilibrium time depends on initial concentrations of Pb(II) ions. The n-HAp nanorod shows the maximum adsorption for the first 5 min and thereafter the equilibrium time was established at 20 min for 20 mg/L of adsorbate. The maximum initial concentration of 100 mg/L attain the equilibrium time at 70 min as shown in Fig 9 (b). The Pb (II) adsorptions capacity of spheres like n-HAp in Fig 10 (d) shows the rapid increase in the adsorption for first 5 min and thereafter the equilibrium time was observed at 80 min

for all the initial concentrations of adsorbate. These results confirms the adsorption of Pb (II) ions can be attained rapidly by nanorods like n-HAp compared with the nanospheres which presents a contact time of 80 min to achieve adsorption equilibrium. The fast rate of adsorption equilibrium between 5 and 70 min for HAp nanorods should be used as a good adsorbent material for the removal of heavy weight metal ions from aqueous solutions.

Adsorption Kinetics Study:

Pb (II) adsorption kinetic analyses were performed with different morphologies of rod- and sphere-like n-HAp using theLagergren's first order rate equation as described in equation (1).

$$\log(q_e - q_t) = \log q_e - \frac{K_1}{2.303} t \qquad (1)$$

Whereq_e andq_t are the amounts of metal ions adsorbed (mg/g) at equilibrium and any given time t (min) respectively. $K_1$is the pseudo-first order reaction rate constant for adsorption (min^{-1}). The values of the q_e and K_1, were calculated from the slope and intercept of the plots of $log(q_e - q_t)$ versus time (t) as shown in Fig.10 (a) & (c).
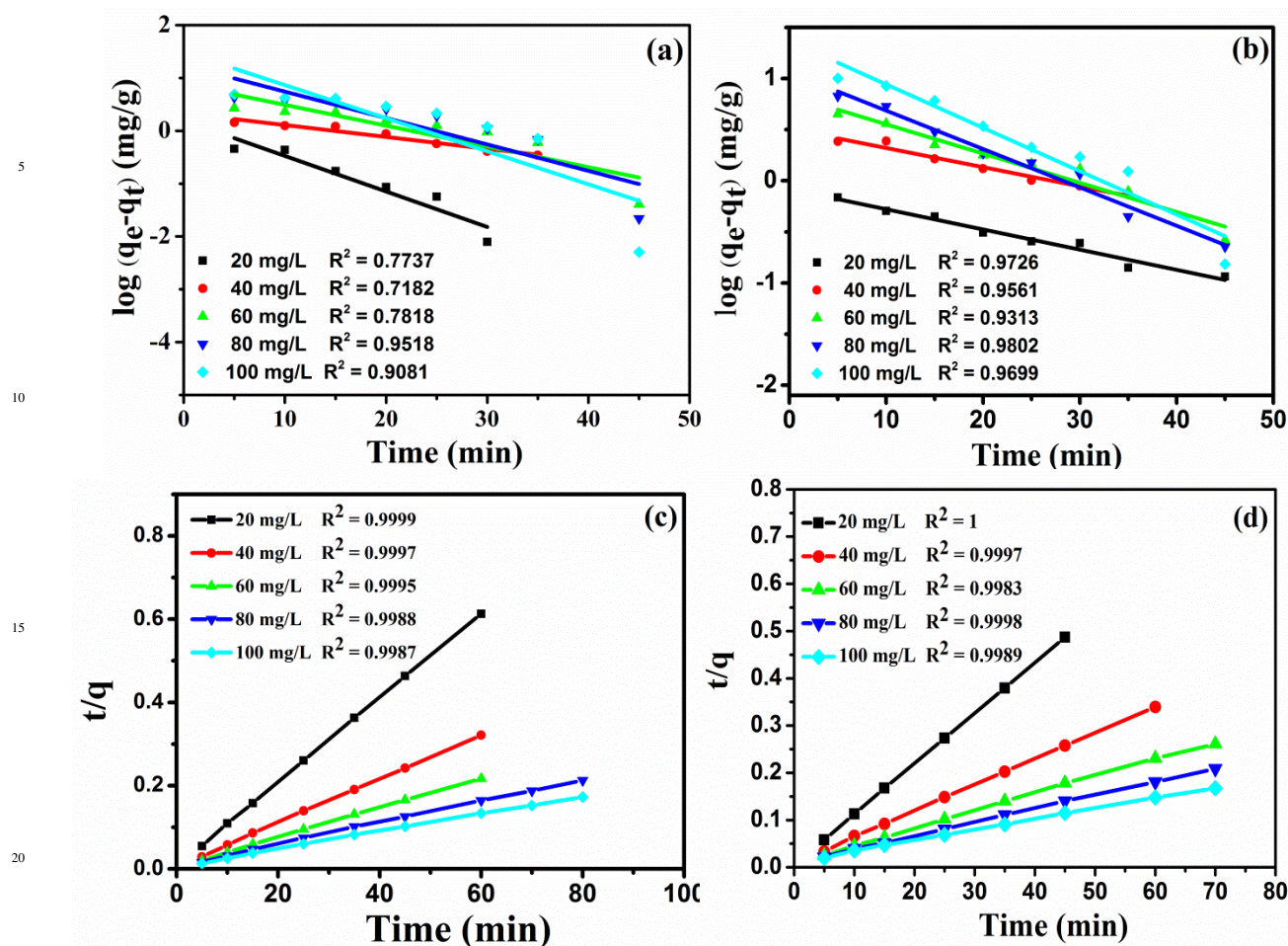
Fig.10 Linear fit of experimental data obtained using pseudo first and second order model for the adsorption of Pb (II) ions for (a) and (c) n-HAp nanorods and (c) and (d) n-HAp nanosphere.

The pseudo second order kinetic model can be represented as equation (2).[34,35]

$$\frac{t}{q_t} = \frac{t}{q_e} + \frac{1}{K_2 q_e^2} \qquad (2)$$

Where K_2 is the equilibrium rate constant of pseudo second order adsorption (g mg^{-1} min^{-1}). The values of K_2 and q_e were calculated from the plots of t/q versus t as shown in Fig 10 (b) & (d). The pseudo-first order kinetics, the experimental data significantly deviates from linear fit and this was evident by the low correlation values. It suggests the pseudo-first-order kinetic model is not suitable for describing the kinetics of the adsorption process. The correlation coefficients were closer to unity for pseudo-second order kinetics than that for the pseudo-first order kinetics. This indicates the adsorption of Pb (II) on the nanorods and nanospheres of HAp nanostructures follow the pseudo-second order kinetic model.

Adsorption Isotherm:

Adsorption isotherms are mathematical models that describe the distribution of the adsorbate species between liquid andadsorbent based on a set of assumptions that are mainly associated to the homogeneity/heterogeneity of adsorbents and

type of coverage and probability of interaction between theadsorbate species.The adsorption data of Pb(II) on the n-HAp were used to determine the characteristic adsorption constants by using Langmuir isotherm and Freundlich models. The adsorption isotherm of Langmuir and Freundlich models of Pb (II) ions are shown in Fig 11. The experimental data were fitted based on Langmuir isotherm and Freundlich models to explain the adsorption performances of heavy weight metal ions on theadsorbents

The Langmuir and Freundlichequations can be expressed by the linearized form as:[23,33,34]

$$\frac{C_e}{q_e} = \frac{1}{Q_0 b} + \frac{C_e}{Q_0} \qquad (3)$$

$$\log q_e = \log K_f + \frac{\log C_e}{n} \qquad (4)$$

Where C_e and q_e are the equilibrium concentration (mgL^{-1}) and amount of adsorption at equilibrium (mg g^{-1}). Q_o and b is Langmuir constants related to the theoretical monolayer adsorption efficiency(mg g^{-1}) and energy ofadsorption(L mg^{-1}) respectively.
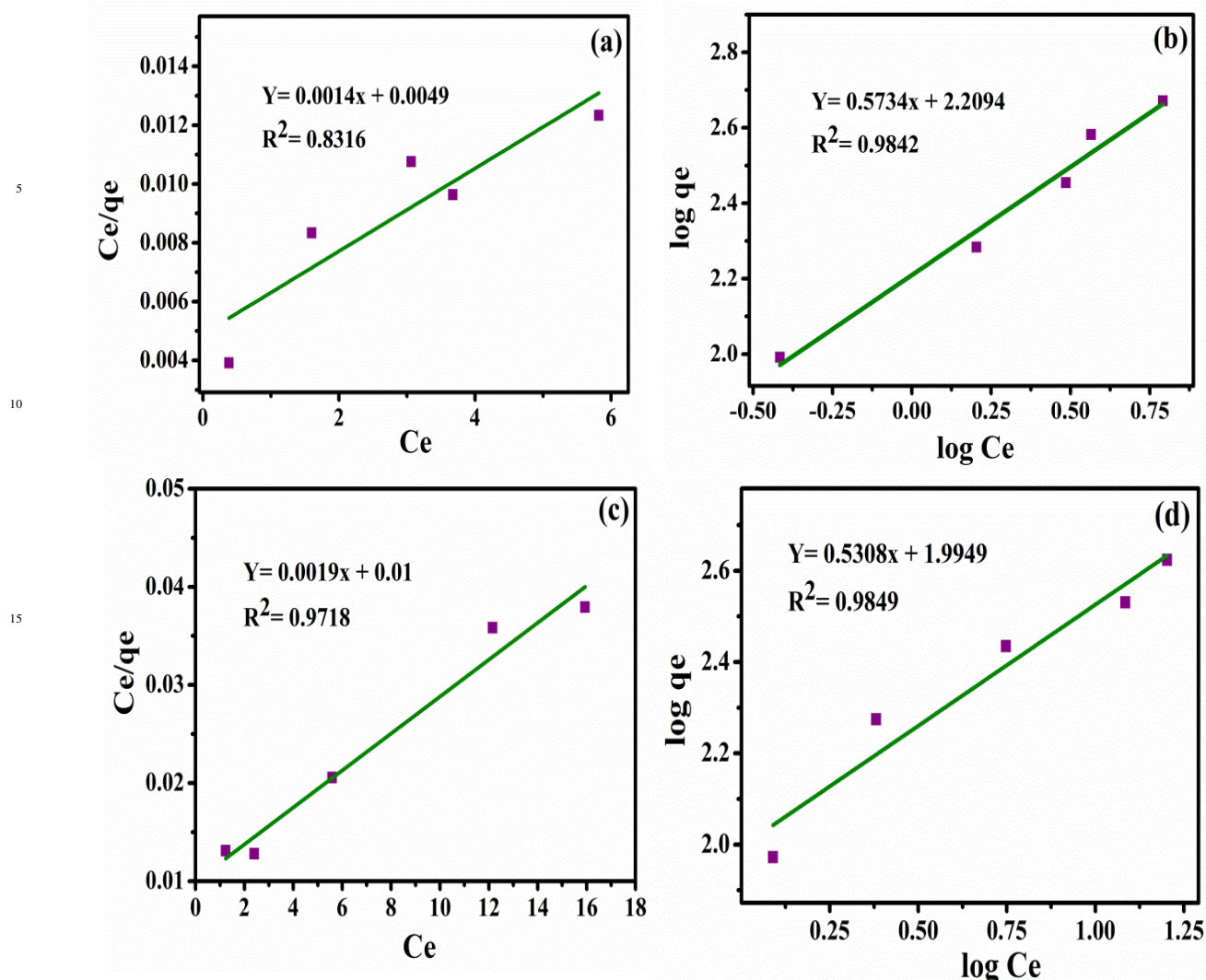
Fig.11 Adsorption isotherms of Pb(II) ions based on Langmuir and Freundlich isotherm for (a) and (b) hydroxyapatite nanorods, (c) and (d) hydroxyapatite nanospheres.
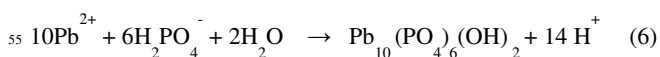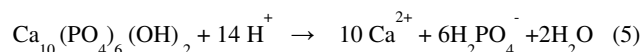
The linear plots of C_e/q_e vs C_e suggest the applicability of the Langmuir isotherms. Values of Q_o and b were determined from the slope and intercepts of the plots. The values of Q_o and b indicate the maximum adsorption corresponds to a saturated monolayer of adsorbate ions on adsorbent surface. The fitted parameters from the experimental data with both Langmuir and Freundlich isotherms were presented in Table 1. The maximum adsorption efficiency (Q_o) observed based on Langmuir model were 714.14 and 526.31 mg/g for the Pb (II) ions for the nanorods and nanospheres of n-HAp respectively.The constants and correlation coefficients of Pb (II) ions on n-HAp nanorods and nanospheres were compared and reported in Table.1 for comparison. It shows the nanorods have maximum adsorption capacity due to the high specific surface area (SSA).The Freundlich isotherm undertakes heterogeneous adsorption due to the diversity of adsorption sites. The Freundlich constants K_f and n were calculated from the linear plot of log q_e vs log C_e and were presented in Table 1. The values of the adsorption isotherm constants n and R^2 indicate the experimental values are well fitted with the Freundlich model. So it confirms the adsorption of Pb (II) ions from aqueous solution by n-HAp and in particular n-HAp nanorods shows good heterogeneous adsorption capacity than the nanospheres. The Pb(II) adsorption

capacity of the HAp nanorods was higher than that of the reported values as presented in Table 2.

Pb(II) Adsorption Mechanism:

The synthesized n-HAp nanorods and nanosphere shows good adsorption capability of Pb (II) ions from aqueous solutions. The adsorption mechanism depends on three factors such as surface adsorption, cation substitution and precipitations. The maximum adsorption of Pb (II) ions was achieved at acidic condition.

The present experimental result shows the maximum removal percentage of 97.5 and 90.5 % for n-HAp nanrods and nanospheres with a pH of 4. The ion exchange mechanism between Pb (II) and HAp can be described as follows:[34,35]

$$Ca_{10}(PO_4)_6(OH)_2 + 14\,H^+ \rightarrow 10\,Ca^{2+} + 6H_2PO_4^- + 2H_2O \quad (5)$$

$$10Pb^{2+} + 6H_2PO_4^- + 2H_2O \rightarrow Pb_{10}(PO_4)_6(OH)_2 + 14\,H^+ \quad (6)$$

The pH is the most important parameters for the adsorption of Pb (II) ions from waste water.

Table 1 Langmuir and Freundlich constants and correlation coefficients for adsorption of Pb (II) on HAp nanorods and nanospheres.

Metal Ions	Langmuir			Freundlich		
	$Q_0 \, (mg \, g^{-1})$	b	R^2	$K_f(mg^{1-1/n}L^{1/n} \, g^{-1})$	n	R^2
Pb (II) on HAp Nanorods	714.14	0.2551	0.8316	161.96	1.7438	0.9841
Pb (II) on HAp Nanospheres	526.31	0.1921	0.9718	98.83	1.8898	0.9849

Table 2 Summary of the Maximum Pb (II) removal capacities by different adsorbents

S.No	Adsorbent	Adsorption Capacity mg g^{-1}	Reference
1	Power activated carbon	20.7	38
2	Fly ash	15.08	39
3	Lichen (Cladoniafurcata)	12.3	40
4	Melocannabaccifera charcoal	10.66	41
5	Coir (Coco nucifera)	18.9	42
6	Nanorods NiO and Ni(OH)$_2$	32 and28	43
	Dandelion-like NiO and Ni(OH$_2$	26 and 33	
7	Ca-deficient HAp	19.96	44
8	Ni@C composite nanostructures	21.4	45
9	HAP Sphere	**526.31**	**Present Study**
10	HAP Rod	**714.14**	**Present Study**

The effect of pH on adsorption was carried out with the range of pH from 2 to 10. The HAp was easily dissolved and releases maximum calcium and phosphate ions in the range of 41 and 62 mg/L and also consumes H^+ ions with a pH of 3 to 4.[35] During the adsorption process, dissolution and re-precipitation takes place. The equation 5 expresses the dissolution of the HAp nanoparticles to the solution containing different initial concentrations of Pb (II) ions of 10 to 50 mg/L at different pH values.The decrease in the pH interestingly improves the adsorption capacity due to the maximum release of phosphate ions from the hydroxyapatite nanoparticles and the maximum Pb (II) ions interact withphosphate ions at pH 4. Further, the concentration of calcium and phosphate ions increases with an increased contact time and the rapid adsorption observed within first 5 min andfurther it reach a small increase and reaches a saturated equilibrium time at 70 min. Most of the calcium and phosphate ions from the n-HAp were released at 60 min.[36]

In the case of n-HAp nanorods and nanospheres show an equilibrium time of 70 and 80 min respectively. Equation 6,describes the precipitation of Pb (II) in the $6H_2PO_4^-$solution andform a new phase of hydroxypyromorphite, $(Pb_{10} \, (PO_4)_6 \, (OH)_2)$ and releases $H^+$and it was confirmed by several reports.[34-37,46]The maximum Pb (II) adsorption capacity (Q_o) of HAp nanorods andnanospheres were of 714.14and 526.31mg g^{-1} respectively. However, at every initial Pb (II) concentration are in the ranging from 20 to 100 mg/L.The adsorption capacity of nanorods is slightly higher than the nanospheres due to the high specific surface area and high pore size distributions that provide large number of adsorption sites. Therefore, the large number of adsorption sites relatively increases the adsorption of Pb (II) ions on the HAp nanorods.

4. CONCLUSIONS

In summary, the nanorods and nanospheres of HAp were prepared by hydrothermal process by suitably adjusting the concentrations of soft templates CTAB and PEG. The CTAB promotes the nucleation growth on facial *c*-axis and the hydrothermal reaction temperature influences the crystallinity and controls the size and shape of the HAp nanorods. The possible formation mechanism explains the role of PEG concentration on the formation of spindle, rice and spherical like morphologies of n-HAp. Finally, the nanospheres were combined to form the chain like morphology with PEG as only surfactant. The strong electrostatic interaction between Pb(II) and n-HAP at various pH, contact time and adsorbate concentration pays an vital role in adsorption mechanism. The maximum adsorptions capacities were found to be 714.14 and 526.31mg g^{-1}respectively for the n-HAp nanorods and on nanospheres respectively. The pseudo-second order kinetic model was fit rather that the first order. Langmuir and Freundlich adsorptions models were applied to describe the equilibrium isotherms. These nanorods and nanospheres of n-HAP could achieve the a rapid removal of Pb(II) removal. These HAp nanorod and nanosphere have promising and excellent adsorption capacity and thereby it can be used in environmental remediation process.

NOTES AND REFERENCES

ªDepartment of Nanoscience and Technology, Bharathiar University, Coimbatore 641 046, India
10 *ᵇDepartment of Environmental Sciences, Bharathiar University, Coimbatore 641 046, India*
*Corresponding author, e-mail: ponpandian@buc.edu.in,
Phone: + 91-422-2428423.

15 1. S. V. Dorozhkinand M. Epple, *Chem. Int. Ed.*2002,**41**, 3130.
2. J.H. Shepherd, D.V. Shepherd and S.M. Best*, J.Mater.Sci.:Mater.Med.*, 2012, **41**2335-2347.
3. K.W.Wang, L.Z. Zhou, Y. Sun, G.J. Wu, H.C.Gu, Y.R. Duan, F.Chen and Y.J.Zhu, *J. Mater. Chem.*, **2010, 20**, 1161.
20 4. S.D. Jiang, Q.Z. Yao, G.T.Zhou and S.Q. Fu., *J. Phys. Chem. C*, 2012, **116**, 4484-4492.
5. X.Y. Zhao, Y. J. Zhu, F. Chen, B. Q. Lu, C. Qi, J. Zhao and J. Wu., *CrystEngComm.*, 2013,**15**, 7926-7935.
6. F.Chen, Q.L.Tang, Y.J.Zhu, K.W.Wang,M.L.Zang, W.Y.Zhai and 25 J.Chang, *Act Biomater.*,2010,**6**, 3013-3020.
7. H. C. Wu, T. W. Wang, J. S. Sun, W. H. Wang and F.H.Lin., *Nanotechnology*, 2007,**18**,165601.
8. S.Bose, S.K.Saha, *J. Am. Ceram. Soc.*, 2003, **86**, 1055.
9. M .Y.Abyaneh.,*J ElectroanalChem.*, 2002,**530**, 82–88.
30 10. M.P. Ferraz, F.J. Monteiro and C.M. Manuel., *Journal of Applied Biomaterials &Biomechanics.*, 2004,**2**, 74-80.
11. M. Sadat-Shojai., J .*Iran. Chem. Soc.*, 2009,**6**,386-392.
12. I. S. Neira, F .Guitia´n, T. Taniguchi, T .Watanabe and M .Yoshimura.., *J. Mater. Sci*., 2008, **43**,2171–2178.
35 13. I.S. Neira, Y.V. Kolen'ko, O.I. Lebedev, G. V. Tendeloo, H. S. Gupta, F. Guitia´n, and M. Yoshimura., *Crystal Growth & Design*, 2009, **9**, 466-474.
14. M.Y. Ma, Y.J. ZhuandS.W.Cao., *J. Mater. Chem.*, 2008, **18**, 2722–2727.
40 15. X. Guo, W. Wang,G. Wu, J.Zhang, C. Mao, Y. Deng and H. Xi., *New J. Chem.*, 2011,**35**,663–671.
16. H. Zhang, M. Liu, H. Fan and X.Zhang.,*Cryst. Growth Des.* 2012,**12,** 2204–2212.
17. A.Wang, H .Yin, D. Liu,H.Wu, Y .Wada, M.Ren, Y.Xu. T. Jiang and 45 X.Cheng., *Appl. Surf. Sci*. 2007,**253** ,3311–3316.
18. Y.T.Huang, M. Imura, Y. Nemoto, C. H. ChengandY. Yamauchi.,*Sci. Technol. Adv. Mater*.,2011,**12**,045005.
19. E. Mavropoulos, M. H. Rocha-Leão, N.C.C. da Rocha, M.H. Prado da Silva and A.M.Rossi., *J. Mater. Res*.,2007, **22**, 3371-3377.
50 20. X.Y. Zhao, Y.J. Zhu,F.Chen, B. Q. Lu, C.Qi, J. Z.J.Wu., *CrystEngComm.*, 2013,**15** ,7926.
21. W.H.Lee, C.Y.Loo, K.L.Van, A.V. Zavgorodniy and R. Rohanizadeh., *J. R. Soc. Interface*., 2012,**9**,918–927.
22. T. Kawasaki., *J. Chromatogr*., 1991, **544**,147-184.
55 23. K. Rout, M. Mohapatra and S. Anand., *Dalton Trans.*, 2012, **41**, 3302-3312.
24. G. Zhao, X. Ren, X.Gao, X. Tan, J. Li, C. Chen, Y.Huang and X. Wang., *Dalton Trans.*, 2011, **40**, 10945-10952.
25. L. Wang, J. Li, Q. Jiang and L. Zhao., *Dalton Trans.*, 2012, **41**, 4544-60 4551.
26. F. Qin, G. Li, H. Xiao, Z. Lu, H. Sun and R. Chen., *Dalton Trans*., 2012, **41**, 11263-11266.
27. M. Zichuan ,Z. Dongyuan, C. Yongfang, X. Shengtao, W. Yinsu and G. Yuanzhe.,*Dalton Trans*., 2013, **42**, 14261-14267.
65 28. Q.Y.Ma, S.J. Traln, and T.J. Logan., *Environ. Sci. Technol*. 1993,**27**,1803-1810.
29. Y. Liu, D. Hou and G .Wang, *Mater ChemPhys*.,2004,**86**, 69-73.
30. K .Lin, J .Chang and R .Cheng.,*Mater.Lett*, 2007,**61** ,1683.
31. S. Koutsopoulos., *Langmuir*.,2001,**17**,8092-8097.
70 32. Y. Wang, S.Zhang, K.Wei, N.Zhao, J.Chen and X.Wang., *Mater. Lett*.,2006,**60**,1484.
33. F. Y.Wang, H .Wang and J. W Ma., *J. Hazard. Mater*.,2010,**177** ,300–306.
34. T.Suzuki, K.Ishigaki and M.Miyake., *J ChemSoc Faraday* 75 *Trans*.,1984,**80**,3157–3165.
35. Q.Y. Ma,S. J. Tralna, and T.J. Logan., *Environ. Sci. Technol*. 1993,**27**,1803-1810.
36. C.K.Lee, H.S. Kim and J.H.Kwon., *Environ.Eng.Res*.,2005, **10**,205-212.
80 37. X.H. Guo, W.N.Wang, M.J.Wang, C.C.Mao, J.Zhang, F.L.Meng and W.W.Xu., *J NanomedicNanotechnol*., 2012,**3**,1-8.
38. J. Goal, K. Kadirvelu, C. Rajagopal and K.V. Garg.,*J. Hazard.Mater*., 2005, **125**, 211–220.
39. H. Cho, D. Oh and K. Kim., *J. Hazard. Mater*., 2005, **127**, 187–195.
85 40. A. Sari, M. Tuzan, O.D. Uluozlu and M. Soylak.,*Biochem. Eng. J*., 2007, **37**, 151–158.
41. H. Lalhruaitluanga, K. Jayaram, M.N.V. Prasad and K.K. Kumar., *J. Hazard. Mater*.,2010, **175**, 311-318.
42. K. Conrad and H.C.B.Hansen., *Bioresour. Technol.*2007, **98**, 89-97.
90 43. F. Behnoudnia and H. Dehghani., *Dalton Trans*., 2014, **43**, 3471.
44. Z. Zhu, L. Li, H. Zhang, Y. Qiu, and J. Zhao., *Separation Science and Technology*., 2010, **45**, 262-268.
45. Y. H. Ni, L. N. Jin, L. Zhang and J. M. Hong, *J. Mater. Chem.*, 2010, **20**, 6430.
95 46. S. Meski, S. Ziani, and H. Khireddine, Removal of Lead Ions by Hydroxyapatite Prepared from the Egg Shell, *J. Chem. Eng. Data* 2010,**55**,3923-3928.

100

Shape Evolution and Size Controlled Synthesis of Mesoporous Hydroxyapatite Nanostructures and their Morphology Dependent Pb(II) Removal from Waste Water

G. Bharath,[a] A. JagadeeshKumar,[b] K. Karthick,[b] D.Mangalaraj,[a] C.Viswanathan,[a] and N.Ponpandian[a]*

Graphical abstract

Nanostructured hydroxyapatite with tunable morphologies were prepared by suitably adjusting the surfactants and used as an adsorbent for Pb (II) from the waste water.